



CDOM in the source regions of the Yangtze and Yellow Rivers, China: optical properties, possible sources, and their relationships with environmental variables

Dianbao Li¹ · Baozhu Pan¹ · Xing Zheng¹ · Xiaoming Jiang¹ · Gengnan Zhao¹ · Xu Han¹

Received: 23 August 2019 / Accepted: 19 May 2020 / Published online: 10 June 2020
© Springer-Verlag GmbH Germany, part of Springer Nature 2020

Abstract

The source regions of the Yangtze and Yellow Rivers on the Qinghai-Tibet Plateau are extremely important water resources and ecological functional areas in China, and the ecological environment is fragile and sensitive to climate change. Chromophoric dissolved organic matter (CDOM) is an important component that plays a crucial role in the biogeochemical cycle in aquatic ecosystems. However, knowledge of the distribution characteristics of CDOM in this area is limited. In this study, the optical properties, possible sources of CDOM, and their relationships with environmental variables were investigated in the two regions. The results indicated that the CDOM absorption spectra of these two source regions had a high degree of consistency, and the absorption coefficient $a_{CDOM}(355)$ was small, with a mean of $2.07 \pm 1.10 \text{ m}^{-1}$. Two fluorescence components (C1 and C2) were identified and grouped into the humic-like component with parallel factor analysis (PARAFAC) of fluorescence excitation-emission matrices (EEMs), which exhibited highly similar (excitations/emission)_{max} positions between each pair of components in the two regions. Comprehensive CDOM spectral absorption and fluorescence parameters suggested that CDOM was mainly derived from externally input humus, and the source region of the Yellow River showed stronger allochthonous sources. The dissolved organic carbon (DOC) gradients in the water affected the fluorescence intensity and indicated that the humic-like component was an important component of DOC. Water temperature (WT) and turbidity (Turb) positively affected the concentration of CDOM and the ability to absorb light in the aquatic ecosystems. Due to global warming, the rising temperature may lead to an increase in meltwater inflow in the source area and will also bring more external inputs through the runoff.

Keywords CDOM · Optical properties · EEMs–PARAFAC · Possible sources · Multivariate analysis · The source regions of the Yangtze and Yellow Rivers

Introduction

As the key channel connecting terrestrial and marine ecosystems, river systems play a crucial role in carbon transformation from land to the ocean (Regnier et al. 2013; Wehrli 2013; Schefuß

et al. 2016). The flux of carbon in rivers can reflect hydrogeology, climate, land use, vegetation cover, and human activities in the basin. Carbon in rivers mainly originates from the atmosphere, fixed organic carbon by the photosynthesis reaction, terrestrial input by surface runoff, and microbial degradation in rivers (Raymond et al. 2008; Stets and Striegl 2012; Grand-Clement et al. 2014). Dissolved organic matter (DOM) is one of the main forms of carbon in water, with a wide range of molecular weights changes and complex molecular structures, which interact with the physical and chemical behavior of water bodies (Hassett 2006; Williams et al. 2016).

Chromophoric dissolved organic matter (CDOM) is the colored and photoactive fraction of DOM. Due to its strong absorption in the ultraviolet (UV) and visible light regions of the spectrum in aquatic ecosystems, CDOM concentration and composition changes can significantly affect the availability and spectral quality of underwater light fields (Kirk 2011).

Responsible editor: Céline Guéguen

Electronic supplementary material The online version of this article (<https://doi.org/10.1007/s11356-020-09385-w>) contains supplementary material, which is available to authorized users.

✉ Baozhu Pan
zhuzipan@xaut.edu.cn

¹ State Key Laboratory of Eco-hydraulic in Northwest Arid Region of China, Xi'an University of Technology, Xi'an 710048, Shaanxi, China

CDOM absorbs most strongly in the ultraviolet region, so it limits the penetration depth of biologically harmful UV-B radiation (280–320 nm), and protects aquatic organisms against harmful radiation (Stedmon et al. 2000; Huovinen et al. 2003). CDOM is decomposed into small molecular organic matter and inorganic nutrients through photochemical and microbial degradation processes to create conditions for the growth of aquatic organisms such as algae, microorganisms, and aquatic vegetation (Veuger et al. 2004; Osburn et al. 2009; Lapierre and Frenette 2009). However, these processes also release greenhouse gases such as CO₂ and CH₄, which will aggravate global warming (Granéli et al. 1999; Tranvik et al. 2009; Jørgensen et al. 2014). Moreover, the CDOM absorption of visible light competes with algae and aquatic vegetation for photosynthetically available radiation (PAR), which in turn affects the productivity and structure of the aquatic system. (Stedmon et al. 2000; Zhang et al. 2011a). CDOM absorption in the blue region of visible light overlaps with the absorption band of phytoplankton chlorophyll *a* (Chl*a*) and total suspended matter (TSM), which will lead to the inhibition of phytoplankton photosynthesis, a reduction of primary productivity, and interference in the estimation of phytoplankton biomass and TSM concentration by remote sensing (Rochelle-Newall and Fisher 2002; Doxaran et al. 2002; Zhang et al. 2009). CDOM is complex in composition, mainly including humic acid and fulvic acid, which originate from aquatic biological secretions, algae and aquatic vegetation degradation, river inputs from land and marshes, atmospheric wet deposition through rainfall and release from sediment, especially in inland waters (Rochelle-Newall and Fisher 2002; Zhang et al. 2007a; Zhou et al. 2017; Burdige et al. 2004). In addition to the absorption of light, CDOM also fluoresces when excited by light in the UV and blue regions of the spectrum (Stedmon and Markager 2003; Stedmon et al. 2003). As a result, several optical approaches, including absorbance and fluorescence, have been used to reflect the internal and surrounding environment of the water body and can indicate the pollution status of the water body to a certain extent and help identify the origins of CDOM in aquatic ecosystems (Baker 2002; Vahatalo et al. 2005; Hudson et al. 2007).

The Three River Source Region (TRSR) is the source of the Yangtze, Yellow, and Lancang Rivers catchment area, which lies in the hinterland of the Tibetan Plateau, the highest and most extensive plateau in the world (Xu et al. 2018b; Fang 2013). The TRSR is called the “Chinese Water Tower”, and approximately 40 billion m³ of water is transported downstream of the source regions every year (Shao et al. 2017). As the source regions of the first and second largest rivers in China, respectively, the source region of the Yangtze River (TSYaR) and that of the Yellow River (TSYeR) have important ecological functions for water resource conservation and management, biodiversity protection, and ecological security in the Yangtze and Yellow River basins. These source regions

have complex topography and a harsh climate, and the ecological environment is fragile and sensitive to climate change (Liu et al. 2014; Ding et al. 2018; Kensuke et al. 2005). However, in recent decades, due to anthropogenic activities and climate changes, stream flows have reduced, snow-capped glaciers have receded, vegetation coverage has changed, lakes have shrunk, rivers have dried up, and the hydrological environment has changed drastically around the world (Pirmia et al. 2019; Liu et al. 2014; Wang et al. 2001; Shi et al. 2017). In addition, soil and water conservation capacity has declined sharply and grassland productivity has declined, causing serious damage to the ecological environment of the source catchment regions and making it difficult to restore it to health (Xu et al. 2018a, 2018b; Cai et al. 2015; Sheng et al. 2019). Taking the TRSR as an example, the State Council of China approved and implemented “The Three River Source Region Ecological Project” in 2005 to carry out ecological restoration and treatment for the ecological environment. Although this project has had a positive contribution to the restoration and protection of TRSR ecosystems, the ecological environment is still not completely restored (Liu et al. 2013; Jiang et al. 2017). Further, the optical properties of CDOM in TSYaR and TSYeR are largely unknown (Nima et al. 2016).

In this study, the CDOM of the main rivers and typical river segments of TSYaR and TSYeR was investigated. The main objectives were (1) to identify the CDOM spectral absorption characteristics and the fluorescence components in TSYaR and TSYeR; (2) to discuss the possible sources of CDOM; and (3) to explore the relationship between CDOM and environmental variables (potential environmental indicators and influential factors of CDOM). This study provides useful information for the role of CDOM in ecological and biogeochemical processes in TRSR areas. Furthermore, it provides a theoretical basis for water environmental protection and ecological restoration in the source area of rivers.

Materials and methods

Study area

TSYaR and TSYeR are located in the northeastern part of the Qinghai-Tibet Plateau (Fig. 1). The average elevation of these regions is > 4000 m (Wang et al. 2017), and the annual temperature ranges from −5.6 °C in January to 7.8 °C in July (Sheng et al. 2019). Annual rainfall is between 262.2 and 772.8 mm mostly falling as snow and heavy rain (Jiang et al. 2017; Fang et al. 2011), and annual evaporation is 1204–1327 mm (Qian et al. 2006). The source regions of the two river systems extend over approximately 15.8 × 10⁴ km² and 12.2 × 10⁴ km², respectively (Yu et al. 2013).

Fluvial morphology, drainage pattern, and riparian vegetation in TSYaR and TSYeR differ markedly (Yu et al.

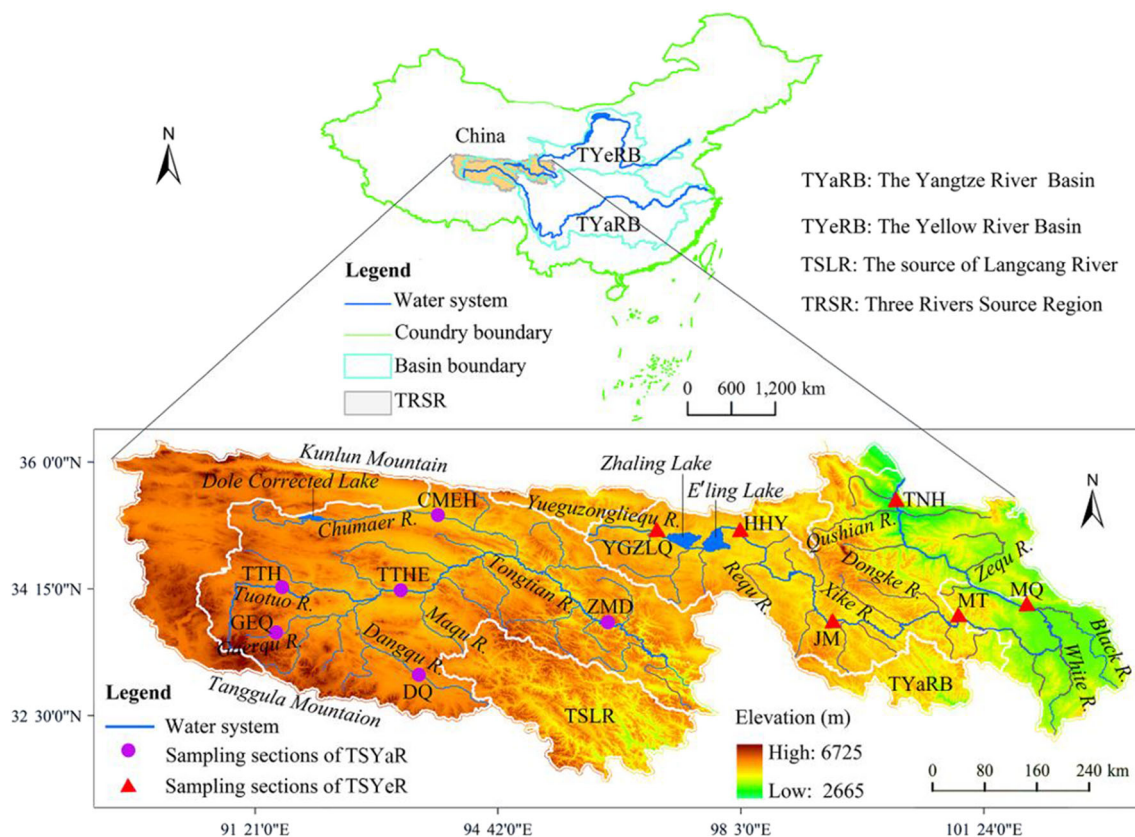


Fig. 1 Locations of sampling segments in the source regions of the Yangtze and Yellow Rivers, China

2013). TSYaR is divided by quasi-parallel low mountains or ridges and developed relatively parallel drainage networks along the area between the low mountains and ridges (Yu et al. 2013; Pan et al. 2013; Li et al. 2018a, 2018b). The river network is dense in TSYaR, and the main tributaries are the Dangqu River in the south, the Tuotuo River in the middle, and the Chumaer River in the north (Wu et al. 2013). TSYeR originates from the Yueguzongliequ Basin of the northern Bayan Har Mountains and flows through the two largest lakes in the region, namely Zhaling Lake and Eling Lake (Li et al. 2013; Blue et al. 2013; Wan et al. 2014). TSYeR exhibits greater variability in morphology than TSYaR. The elevation ranges from 2680 to 6248 m and gradually decreases from the southwest to the northeast (Meng et al. 2016; Wu et al. 2018). The environmental gradient of riparian vegetative development (i.e., the type, quantity and diversity) is associated with interactions between fluvial morphology and the drainage pattern (Yu et al. 2014). The environment is more favorable for vegetation growth in TSYeR than in TSYaR (Yu et al. 2013), and the potential season for vegetation growth in TSYeR is much longer than in the vast majority of TSYaR (Yu et al. 2014). The main differences between the two regions are shown in Table S1.

Field sampling and measurements

A sampling campaign was conducted in TSYeR at the end of July and in TSYaR in early October 2018, i.e., the wet season with relatively abundant water in the two regions (Shen et al. 2003; Feng et al. 2018). A total of 36 water samples were collected, including 18 samples for each region. Six sampling river segments were chosen from sampling in TSYaR and TSYeR, respectively (Fig. 1). Three sampling sites were set in each sampling segment, and the spacing between each site was within the range of 100 to 500 m according to the in situ environment. Surface (0–0.5-m depth) water samples for CDOM absorption, fluorescence, dissolved organic carbon (DOC) concentration, and water quality analysis were collected in a 1-L acid-cleaned polyethylene bottle and held on ice in the field. These water samples were transported to the laboratory as soon as possible and stored in the dark at 4 °C. In addition, at each sampling site, environmental variables were measured after water sample collection. Latitude and longitude were registered using a handheld GPS device (G138BD GPS, UniStrong, China). Water temperature (WT), dissolved oxygen (DO), electrical conductivity (EC), and pH were measured using a multiparameter digital analyzer (HQ30d, HACH, USA). Surface velocity (v) was measured by a

portable flow meter (Flowatch, Switzerland) and turbidity (Turb) was detected using a portable turbidimeter (2100Q, Hach, USA).

Water quality measurements

In the laboratory, water samples for DOC were filtered through 0.45- μm cellulose filters and then measured with a total organic carbon analyzer (Vario TOC, Elementar, Germany). The water samples were analyzed for total nitrogen (TN), nitrate nitrogen (NO_3^- -N), nitrite nitrogen (NO_2^- -N), ammonium nitrogen (NH_4^+ -N), and total phosphorus (TP) by the Standard Methods of Environment Monitoring in China (National Bureau of Environment Protection Editor 2002). TN was determined using a UV spectrophotometric method with alkaline potassium persulfate digestion; NH_4^+ -N concentration was determined using a salicylic acid spectrophotometry method; NO_3^- -N concentration was determined using sulfamic acid UV spectrophotometry; NO_2^- -N concentration was determined using an N-(1-naphthyl)-ethylenediamine spectrophotometric method; and TP concentration was determined using a spectrophotometric method with persulfate potassium digestion.

CDOM absorption measurement and analysis

Water samples for CDOM analysis were first filtered through precombusted (4 h at 450 °C) 0.7- μm GF/F glass filters (Whatman, UK) and then through 0.22- μm membrane cellulose filters (Millipore). The absorption coefficients of CDOM were measured between 200 and 800 nm (path length 1 cm) using a UV–visible spectrophotometer (DR6000, Hach, USA) with Milli-Q water (18.2 $\text{M}\Omega\text{ cm}^{-1}$ resistivity) as a blank. The absorption coefficient (m^{-1}) was calculated from the measured absorbance using Eq. (1) below (Bricaud et al. 1981; Kirk 2011):

$$a_{\text{CDOM}}(\lambda') = 2.303 \times A(\lambda)/r \tag{1}$$

where $a_{\text{CDOM}}(\lambda')(\text{m}^{-1})$ is the uncorrected CDOM absorption coefficient at wavelength λ , $A(\lambda)$ is the absorbance at wavelength λ , and r (m) is the optic pathlength of the quartz cuvette in meters (0.01 m in this study). A correction equation (Eq. (2)) was applied to correct the scattering by residual particles in the filtered sample absorption at 700 nm (Bricaud et al. 1981; Green and Blough 1994):

$$a_{\text{CDOM}}(\lambda) = a_{\text{CDOM}}(\lambda') - a_{\text{CDOM}}(700) \times \lambda/700 \tag{2}$$

The spectral slope of CDOM can be modeled using a single exponential formula according to the nonlinear regression of Eq. (3) (Bricaud et al. 1981):

$$a_{\text{CDOM}}(\lambda) = a_{\text{CDOM}}(\lambda_0) \times \exp[S(\lambda_0 - \lambda)] \tag{3}$$

where $a_{\text{CDOM}}(\lambda_0)$ is the absorption coefficient at reference wavelength λ_0 , which was calculated with 440 nm adopted as the reference wavelength in this study (Kirk 2011; Xu et al. 2018a). S (μm^{-1}), the spectral slope, can reflect small changes in the spectral shape and has been used to explore the biogeochemical process and sources of CDOM. $S_{275-295}$ (wavelength λ is 275–295 nm) values were correlated with CDOM composition or diagenesis and have been widely applied in DOM studies (Li and Hur 2017). The values were calculated using Eq. (3) and can be used to reflect the molecular weight of the CDOM composition and to characterize the source of the CDOM (Helms et al. 2008; Xia et al. 2018). The CDOM concentration was difficult to measure directly because of the complicated composition, $a_{\text{CDOM}}(355)$ is widely used as an indicator of relative CDOM concentration (Kirk 2011; Stedmon et al. 2007b; Zhang et al. 2007b) and was used as a surrogate for CDOM concentration in this study.

Another parameter was derived by absorbance and DOC concentration measurements: $SUVA_{254}$ is defined as the absorbance at 254 nm divided by the DOC concentration (Seritti et al. 1998; Weishaar et al. 2003).

Three-dimensional fluorescence measurements and PARAFAC modeling

CDOM fluorescence excitation-emission matrices (EEMs) were determined using a fluorescence spectrophotometer (FluoroMax-4, Horiba Jobin Yvon, USA). EEM spectroscopy scanning ranges were 200–450 nm for excitation (Ex) and 250–600 nm for emission (Em). Spectral readings were collected in the ratio mode (Sc/Rc) at 5-nm intervals for Ex wavelength and at 1-nm intervals for Em wavelength. The bandpass width of both the Ex and Em was set at 5 nm. Water Raman scatter peaks were eliminated by subtracting a Milli-Q water blank EEMs from the EEM of the measured sample (Li et al. 2018). The Raman scattering of the sample was automatically deducted by the spectrometer system, and the influence of Rayleigh scattering applying factory supplied correction factors (Singh et al. 2010). Inner-filter effects were corrected for the EEM using the measured CDOM absorbance (McKnight et al. 2001; Murphy et al. 2013).

Parallel factor analysis (PARAFAC) is a statistical decomposition technique used to extract the most representative fluorescence components from the complex DOM mixture EEM dataset (Andersen and Bro 2003; Murphy et al. 2013). In this study, PARAFAC of EEM data was conducted using MATLAB 2018a software with the DOMFluor toolbox 1.7 (Bro 1997; Stedmon and Bro 2008). The model can be written as follows:

$$x_{ijk} = \sum_{f=1}^F a_{if} b_{jf} c_{kf} + e_{ijk} \tag{4}$$

where $i = 1, \dots, I; j = 1, \dots, J; k = 1, \dots, K; x_{ijk}$ is the fluorescence intensity of the i th sample at the k th Ex and j th Em

wavelengths; a_{jf} is directly proportional to the concentration of the f th fluorophore in the i th sample; b_{jf} and c_{kf} are estimates of Em and Ex spectra (loadings) of f th fluorophore at wavelength j and k , respectively; F is the number of fluorescence components; and e_{ijk} is the residual noise, which represents unexplained variability in the model.

Due to the SNR (signal-to-noise ratio), the EEM datasets with Ex wavelength less than 250 nm and Em wavelength less than 300 nm were excluded from the calculation of PARAFAC. Considering that the different sampling times and the fluorescence components may differ in the two regions, the EEM data of the two regions were performed by PARAFAC, respectively. According to the PARAFAC results, 2 TSYaR and 1 TSYeR samples were removed because of possible problems. Finally, 16 EEM datasets for TSYaR and 17 EEM datasets for TSYeR were analyzed using PARAFAC modeling separately and were used in this study. Determination of the number of components was performed by split-half analysis and analysis of residuals and loadings (Stedmon et al. 2003). Several fluorescence parameters were used to quantitatively describe and distinguish the fluorescence characteristics of CDOM. The fluorescence index (FI) is defined as the ratio of the Em intensity at 470 nm to that at 520 nm, obtained at Ex 370 nm (Cory and McKnight 2005); the biological index (BIX) is defined as the ratio of Em intensity at 380 nm to that at 430 nm, obtained at Ex 310 nm (Huguet et al. 2009); the humification index (HIX) is defined as the ratio of two spectral regions (435–480 nm and 300–345 nm) from the Em spectrum, obtained at Ex 254 nm (Huguet et al. 2009) (since the bandpass width of Ex was set at 5 nm, we used the value of Ex at 255 nm).

Statistical analyses

The $S_{275-295}$ values of CDOM absorption were obtained using a nonlinear least square regression (Loiselle et al. 2009). Linear discriminant analysis (LDA) was performed using CDOM absorption spectral parameters ($a_{CDOM(355)}$, $SUVA_{254}$, $S_{275-295}$), fluorescence parameters (FI , BIX , HIX), and the percentage of the fluorescence components ($C1(\%)$ and $C2(\%)$) for the sake of classification and dimensionality reduction. Relationships between CDOM absorption spectral variables ($a_{CDOM(355)}$, $SUVA_{254}$, $S_{275-295}$), $C1(\%)$ and $C2(\%)$, the corresponding fluorescence intensity ($I1$ and $I2$) of the fluorescence components ($C1$ and $C2$), the fluorescence index (FI), biological index (BIX), humification index (HIX), and environmental variables (Elevation, WT, DO, EC, pH, v , Turb, DOC, TN, NO_3^- -N, NO_2^- -N, NH_4^+ -N, TP) were determined by Spearman's correlation analysis.

PARAFAC and graphs of CDOM fluorescence components constructed with MATLAB 2018a software. Distribution maps of segments and sampling sites were generated with ArcGIS 10.2 software. The mean, standard

deviation, t test, LDA, Spearman's correlation analysis, and other graphs were generated with Rstudio 1.1.463 (R 3.5.1 version) software (<http://www.r-project.org/>). “*”, “**,” and “***” were considered statistically significant at the levels of 0.05, 0.01, and 0.001 (two-tailed), respectively.

Results

Environmental variables of TSYaR and TSYeR

The WT ranged from 0.3 to 6.2 °C and 4.7 to 21.4 °C in TSYaR and TSYeR, respectively. The WT in TSYeR generally increased with decreasing altitude (Table 1). The average concentrations of DOC were 5.13 ± 1.68 and 6.21 ± 1.78 mg L⁻¹ in TSYaR and TSYeR, respectively, and there was no significant difference between the two regions ($p > 0.05$). The DO, pH, EC, and Turb showed no significant difference between the two regions ($p > 0.05$). In terms of the spatial distribution of river segments in each region, Turb and v tended to increase with decreasing elevation, while there were no obvious spatial distribution patterns for DO, pH, and EC. The water quality of the two regions was good, and some water quality indexes reached the type II–III water quality standard in the “Environmental Quality Standards for Surface Water of China (GB3838-2002).” The concentration of TN in TSYeR (1.72 ± 0.66 mg L⁻¹) was significantly higher than that in TSYaR (0.87 ± 0.27 mg L⁻¹) ($p < 0.05$), while other chemical indicators (NO_2^- -N, NH_4^+ -N, TP) did not differ significantly between the two regions. The concentrations of TN ($0.72 \sim 2.71$ mg L⁻¹), NH_4^+ -N ($0.07 \sim 0.32$ mg L⁻¹), and TP ($0.14 \sim 0.29$ mg L⁻¹) generally increased from the upper mainstream to the lower segments in TSYeR, while they had no obvious spatial distribution regularity in TSYaR.

CDOM absorption spectral features

The absorption spectra demonstrated that the CDOM absorption coefficient decreased with increasing wavelength in an approximately exponential manner from the ultraviolet to the visible light waveband in TSYaR and TSYeR indicating a range of CDOM concentrations (Fig. 2). The absorption coefficient in the visible light waveband was small, especially after the wavelength reached 600 nm, the absorption coefficient gradually approached zero. In general, the CDOM absorption coefficient of TSYeR was significantly higher than that of TSYaR at wavelengths less than 643 nm ($p < 0.05$), which indirectly reflected the differences in CDOM concentration between the two regions.

The larger $a_{CDOM(355)}$ value, the higher the CDOM concentration of the corresponding sample. Figure 3A and B show the spatial variation of CDOM absorption coefficients

Table 1 Mean and standard deviation (SD) of environmental variables in TSYaR and TSYeR

Region	Segment	WT (°C)	DO (mg L ⁻¹)	EC (μs cm ⁻¹)	pH	v (m s ⁻¹)	Turb (NTU)	DOC (mg L ⁻¹)	TN (mg L ⁻¹)	NO ₃ ⁻ -N (mg L ⁻¹)	NO ₂ ⁻ -N (mg L ⁻¹)	NH ₄ ⁺ -N (mg L ⁻¹)	TP (mg L ⁻¹)	
TSYaR	GEO	Mean	7.90	751.00	7.20	0.23	25.13	5.44	0.96	0.62	0.03	0.05	0.02	
		SD	0.16	4.08	0.25	0.05	0.56	2.28	0.30	0.23	0.00	0.02	0.00	
	DQ	Mean	1.50	1817.00	7.37	0.33	161.00	5.41	0.91	0.54	0.01	0.12	0.10	
		SD	0.29	35.44	0.09	0.05	0.82	1.68	0.04	0.02	0.00	0.03	0.02	
	TTH	Mean	3.70	2054.00	6.62	0.95	132.50	6.67	0.87	0.54	0.02	0.06	0.13	
		SD	0.00	1.00	0.11	0.15	2.50	2.20	0.03	0.01	0.00	0.01	0.01	
	TTHE	Mean	1.13	1836.00	7.76	0.37	169.33	4.42	0.91	0.41	0.02	0.24	0.08	
		SD	0.17	0.13	58.29	0.12	0.05	3.68	0.40	0.15	0.01	0.16	0.01	
	CMEH	Mean	5.55	6.91	314.50	6.32	0.70	706.50	4.48	0.46	0.26	0.02	0.05	0.61
		SD	0.15	0.11	5.50	0.26	0.00	0.50	0.77	0.03	0.01	0.01	0.00	0.02
ZMD	Mean	6.27	7.51	1540.67	8.27	0.97	371.33	4.67	0.98	0.64	0.02	0.06	0.20	
	SD	0.09	0.02	2.62	0.15	0.21	1.25	0.81	0.05	0.03	0.00	0.02	0.05	
	Mean	5.80	7.22	626.00	8.04	0.65	104.70	6.88	0.98	0.12	0.03	0.08	0.16	
	SD	0.99	0.14	24.10	0.17	0.02	4.24	0.97	0.04	0.01	0.00	0.01	0.01	
HHY	Mean	16.03	5.38	1031.33	7.86	0.46	12.40	5.63	0.75	0.25	0.05	0.10	0.22	
	SD	0.61	0.12	44.79	0.36	0.06	0.79	0.50	0.03	0.01	0.00	0.00	0.02	
JM	Mean	15.67	6.31	407.33	7.75	0.89	39.30	7.39	1.98	0.21	0.05	0.12	0.16	
	SD	0.12	0.15	5.79	0.05	0.04	2.77	2.78	0.15	0.03	0.00	0.00	0.01	
MT	Mean	19.07	5.61	369.67	7.32	0.82	108.63	5.70	2.14	0.32	0.06	0.15	0.21	
	SD	0.52	0.04	9.03	0.05	0.01	31.48	1.49	0.13	0.09	0.01	0.01	0.01	
MQ	Mean	20.50	5.14	295.00	7.69	0.56	144.00	6.93	2.49	0.18	0.05	0.31	0.25	
	SD	0.40	0.17	1.00	0.12	0.01	8.00	1.42	0.22	0.00	0.00	0.00	0.01	
TNH	Mean	21.20	6.25	378.00	8.39	1.11	475.67	4.96	2.22	0.16	0.06	0.20	0.29	
	SD	0.16	0.32	2.94	0.13	0.03	10.37	1.08	0.18	0.05	0.00	0.03	0.00	

WT water temperature, DO dissolved oxygen, EC electrical conductivity, v surfer velocity, Turb turbidity, DOC dissolved organic carbon, TN total nitrogen, NO₃⁻-N nitrate nitrogen, NO₂⁻-N nitrite nitrogen, NH₄⁺-N ammonium nitrogen, TP total phosphorus

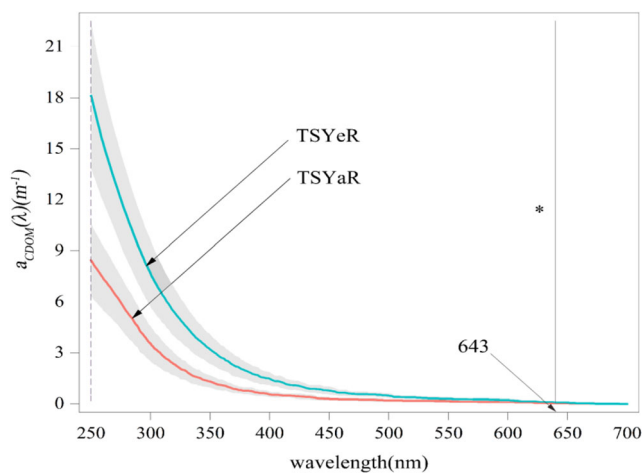


Fig. 2 Averages of CDOM absorption spectra (LightCoral (no. F8766D) and DarkTurquoise (no. 00BFC4) solid lines), plus standard deviations (gray-shaded area) measured in the source regions of the Yangtze and Yellow Rivers, China. Asterisk denotes being statistically significant at the levels of 0.05

($a_{CDOM(355)}$) in TSYaR and TSYeR, ranging from 0.57 to 4.49 m^{-1} , with a mean of $2.07 \pm 1.10 m^{-1}$; the coefficient of variation was 53.1%. The $a_{CDOM(355)}$ values of TSYaR and TSYeR had similar spatial variation characteristics: the $a_{CDOM(355)}$ value increased gradually from the upper branch to the mainstream (except in the TTH segment) in TSYaR and from the upper part of the mainstream to the lower segments in TSYeR (except in the HHY and TNH segments) (Fig. 3A). The mean absorption coefficient ($a_{CDOM(355)}$) of TSYeR ($2.97 \pm 0.83 m^{-1}$) was significantly higher than that of TSYaR ($1.18 \pm 0.37 m^{-1}$) ($p < 0.001$) (Fig. 3B).

The values of $SUVA_{254}$, which indicated the aromaticity and reactivity of CDOM, were different across all study segments (Fig. 3C, D), ranging from 0.66 to 4.45 $L^{-1} m^{-1} mg$, with a mean of $2.20 \pm 0.96 L^{-1} m^{-1} mg$. The $SUVA_{254}$ value and $a_{CDOM(355)}$ had similar spatial variation characteristics, except that the values in the Maqu River segment (MQ) were lower than those in the Mentang (MT) and Tangnaihah (TNH) segments in TSYeR. Similarly, the spatial mean $SUVA_{254}$ exhibited a marked difference between the two regions, and the mean $SUVA_{254}$ value of TSYeR ($2.85 \pm 0.8 m^{-1}$) was significantly higher than that of TSYaR ($1.46 \pm 0.26 m^{-1}$) ($p < 0.001$) (Fig. 3D).

Additional optical characteristics and the distribution of spectral slope $S_{275-295}$ values (wavelength at 275–295 nm) also showed differences in organic matter quality between all study segments. The $S_{275-295}$ mean value was $17.19 \pm 1.86 \mu m^{-1}$ and values ranged from 12.37 (JM) to 24.27 μm^{-1} (GEQ). The spatial distribution of $S_{275-295}$ values did not exhibit an obvious trend in segments of TSYaR and TSYeR (Fig. 3E). From the regional perspective, however, the mean $S_{275-295}$ value of TSYaR ($18.25 \pm 3.08 \mu m^{-1}$) was significantly higher than that of TSYeR ($16.13 \pm 1.89 \mu m^{-1}$) ($p < 0.05$) (Fig. 3F).

Overall, when all twelve river segments were considered together, it was found that the variation in the $a_{CDOM(355)}$ and $SUVA_{254}$ values generally showed a consistent tendency (Fig. 3A, C), while the $S_{275-295}$ values showed no clear regularity (Fig. 3E). The distributions of $a_{CDOM(355)}$ and $SUVA_{254}$ values were relatively concentrated in TSYaR and scattered in TSYeR (Fig. 3B, D), and the distributions of $S_{275-295}$ values in the two regions were opposite (Fig. 3F).

CDOM EEM–PARAFAC components and qualitative indexes

The EEM data of all samples measured in the two regions were analyzed by the PARAFAC method, respectively. The two components (C1 and C2) of the two regions were identified and subjected to a split-analysis validation procedure and a random assignment test, and the simulation degree exceeded 99.5%. These two components could be grouped into one category: humic-like component, which had highly similar (Ex/Em)max positions between each pair of components in the two regions (Table S2; Fig. 4). The characteristics of the two components were similar to those of CDOM previously reported in other aquatic environments (Table S2). C1 showed two excitations (Ex) maxima at 260 and 365 nm, with one emission (Em) maximum at 538 nm (TSYaR) or 539 nm (TSYeR), and C2 displayed two Ex maxima at ≤ 250 and 310 nm, with one Em maximum at 412 nm (TSYaR) or 416 nm (TSYeR). The fluorescence components were similar; however, the average proportions of the components were different in the two regions. In TSYaR, C1 and C2 accounted for 51.86% and 48.14%, respectively, while the corresponding proportions in TSYeR were 47.71% and 52.28%. Of course, what needs to be pointed out in this study was that although the two components were identified using the PARAFAC model, this did not mean that only two types of fluorophores were present in these samples.

The fluorescence index (FI) in our study varied from 1.50 to 1.79, with a mean of 1.63 ± 0.07 . The average FI in GEQ (1.73 ± 0.06) was significantly higher than that in the TTH (1.65 ± 0.02) ($p < 0.05$), but the values were not significantly different from those of other river segments in TSYaR ($p > 0.05$) (Fig. 5A). In TSYeR, the average FI in the HHY (1.67 ± 0.01) was the highest and was significantly different from other river segments ($p < 0.05$), and the lowest FI was found in the MQ segment (1.51 ± 0.02) (Fig. 5A). Regionally, the FI in TSYaR was significantly higher than that in TSYeR ($p < 0.001$) (Fig. 5B). The biological index (BIX) within all sampling segments ranged from 0.64 to 0.84, with a mean of 0.75 ± 0.06 . Relatively high BIX values were found in the CMEH (0.81 ± 0.02) and ZMD (0.82 ± 0.02) river segments, which were significantly higher than that in the TTH (lowest) river segment ($p < 0.05$), and other river segments in TSYaR were not significantly different from each other (Fig. 5C). The

BIX values of the HHY and MT river segments were significantly higher than those of other river segments ($p < 0.05$) but were not significantly different from each other ($p > 0.05$) (Fig. 5C). From a regional perspective, a significantly higher mean *BIX* was recorded in TSYaR (0.80 ± 0.01) than in TSYeR (0.71 ± 0.03) ($p < 0.001$) (Fig. 5D). The spatial distribution of the humification index (*HIX*) was different from that of *FI* and *BIX* in this study area. The highest *HIX* was found in the TTH (4.77 ± 0.41) and the lowest in the CMEH (2.72 ± 0.01). The *HIX* values of the JM and TNH river segments were relatively high, and the lowest value was recorded in HHY (2.19 ± 0.28) (Fig. 5E). Overall, the mean *HIX* value of TSYeR (4.69 ± 1.64) was significantly higher than that of TSYaR (3.76 ± 0.66) ($p < 0.05$) (Fig. 5F).

The LDA results were a good representation of the differences in CDOM between TSYaR and TSYeR (Fig. 6). The first two LDA axes (LD1, 91.45%; LD2, 3.51%) explained 94.96% of the total variability in the CDOM spectral parameters. The first LD1 axis showed relatively high loadings for $a_{CDOM}(355)$ and *FI*. The *BIX*, *C1*(%), and *C2*(%) had loadings on the second LD2 axis, which only accounted for 3.51% of the variance. Most of the segments of TSYaR were clustered on the negative side of the LD1 axes, whereas the segments of TSYeR were clustered on the positive side of the LD1 axes. To some extent, the LDA results further showed the differences in CDOM between TSYaR and TSYeR.

Correlations between CDOM and environmental variables

Multivariate analyses were performed on CDOM parameters and environmental variables to demonstrate the influential factors of the water physicochemical properties for CDOM in this study area.

Spearman's correlation analysis provided additional insight into the relationship between the CDOM parameters and environmental variables. There were different scale effects for the two regions in this study. In TSYaR, Spearman's correlation analysis showed that DOC had a significant positive correlation with fluorescence intensity I1 ($r = 0.832$, $p < 0.001$) and I2 ($r = 0.862$, $p < 0.001$), and had a significant negative correlation with *FI* ($r = -0.785$, $p < 0.001$); EC, NO_3^- -N, and DOC have similar effects on CDOM, but the significance was relatively lower (Fig. 7a); In addition, there were significant positive correlations between *v*, WT, TP, Turb, and the CDOM absorption coefficients $a_{CDOM}(355)$ and $SUVA_{254}$; and TN and DO had a significant negative correlation with $S_{275-295}$ ($r = -0.564$, $p < 0.01$) and $a_{CDOM}(355)$ ($r = -0.512$, $p < 0.01$), respectively (Fig. 7a).

Spearman's correlation analysis of the CDOM parameters and environmental variables in TSYeR is shown in Fig. 7b. DOC was significantly positively correlated with fluorescence intensity I1 ($r = 0.539$, $p < 0.05$) and I2 ($r = 0.657$, $p < 0.01$),

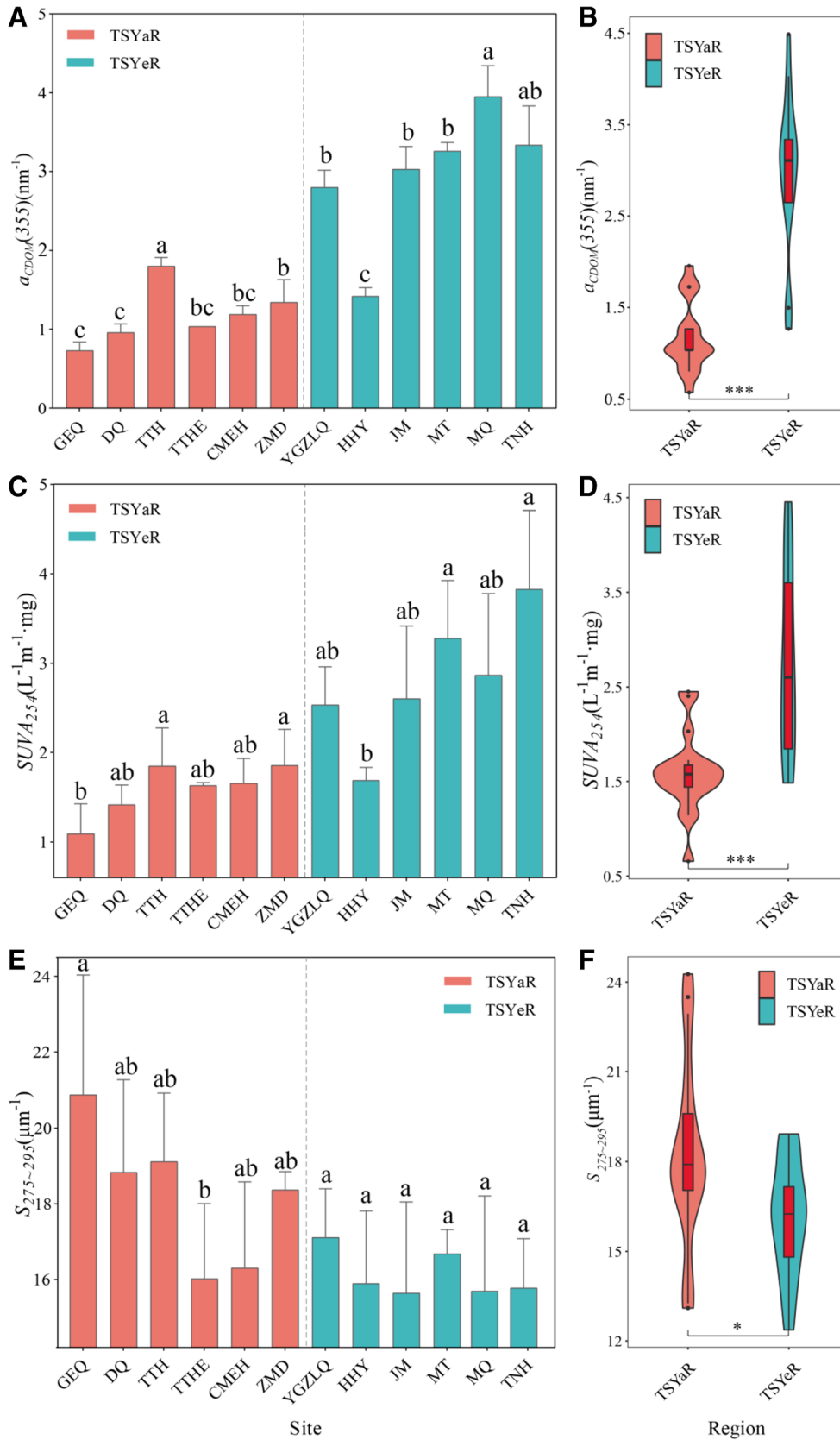
and significantly negatively correlated with $SUVA_{254}$ ($r = 0.613$, $p < 0.01$); WT, Turb, and NH_4^+ -N were positively correlated with $a_{CDOM}(355)$ and $SUVA_{254}$ and negatively correlated with *FI*, while EC and Elevation were opposite to these water quality parameters. NO_3^- -N had significant negative correlation with *HIX* ($r = -0.540$, $p < 0.05$) and a significant positive correlation with *BIX* ($r = 0.618$, $p < 0.01$) (Fig. 7b).

Discussion

CDOM optical properties in TSYaR and TSYeR

Due to the complex chemical composition of CDOM, its concentration is generally expressed by the absorption coefficient at a certain wavelength (Kirk 2011; Stedmon et al. 2007b), such as $a_{CDOM}(355)$ in this paper. Studies have shown that absorption is near the limit or is negative for wavelengths longer than 350 nm for some very clear water bodies, and absorption was significantly positively correlated with TN, TP, Chl*a*, and the trophic state index (TSI) (Zhang et al. 2018). The disturbance caused by Human activity was relatively low, and some water quality indexes reached to the type II~III water quality standard in the two regions. This was one of the reasons for the low CDOM concentration (with a mean of $2.07 \pm 1.10 \text{ m}^{-1}$), and values were even negligible (Shang et al. 2018). $SUVA_{254}$ reflects the proportion of aromatization in the CDOM molecular structure (Weishaar et al. 2003) and indirectly characterizes the absorption capacity of CDOM for light (Zhang and Qin 2007; Morris and Hargreaves 1997). In this study, the average $SUVA_{254}$ values in the two source regions were significantly different (Fig. 3C, D), indicating that the concentration of aromatic substances in CDOM was different, and the ability to absorb light was also different. It should be pointed out that the sampling times of the two regions were different. Although the water was abundant in the respective sampling periods, environmental variables differed with respect to the temporal distribution (Table 1). From the

Fig. 3 Bar plots and violplot box plots showed the spatial distribution of CDOM absorption spectral parameters in all sections and two regions of TSYaR and TSYeR, respectively. (A, B) spatial variation of absorption coefficients at 355 nm ($a_{CDOM}(355)$); (C, D) spatial variation of carbon-specific CDOM absorption at 254 nm ($SUVA_{254}$); (E, F) spatial variation of the spectral slope for 275~295 nm ($S_{275-295}$). Red box boundaries in violplot box plots indicate the 25th and 75th percentiles; the whiskers represent the maximum/minimum values except for outliers; the inner horizontal blacked line is the median; the outside violin plot showed the data distribution and its probability density. Different lowercase letters above the bar plots mean significant difference at the 0.05 level. Single and double asterisks denote being statistically significant at the levels of 0.05 and 0.001, respectively



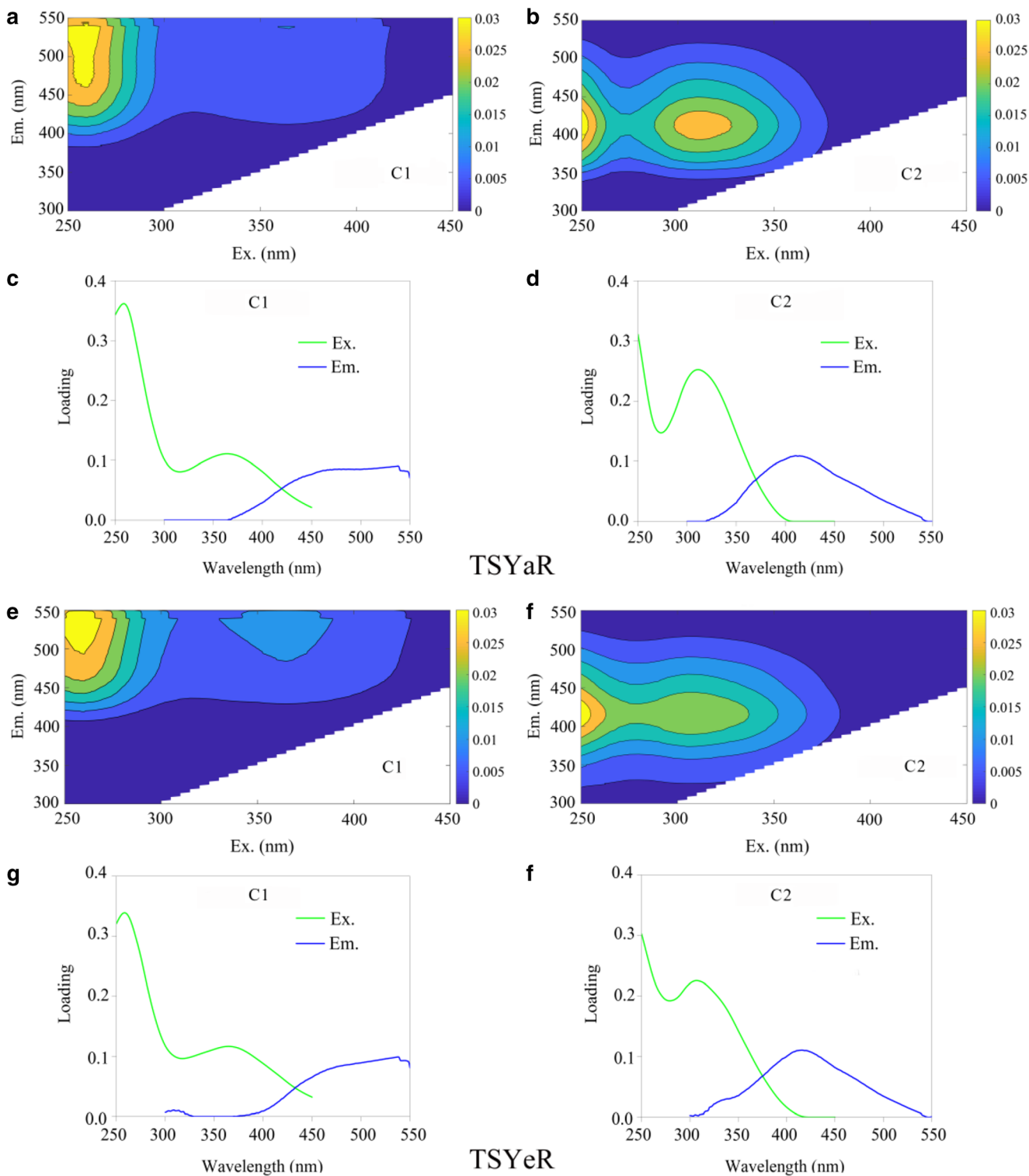


Fig. 4 The two fluorescence components were found from the results of PARAFAC modeling. Contour plots (a, b, e, f) present spectral shapes of excitation and emission, positions of their maxima are given in Table S2. The loadings (c, d, g, h) derived from the two components PARAFAC

model using split-half validation technique. Solid green lines represent Ex loadings for the whole dataset and solid blue lines represent Em loadings for the whole dataset

perspective of the CDOM composition, combined with the CDOM absorption parameters values ($S_{275\sim 295}$), it was found that greater $SUVA_{254}$ resulted in lower

$S_{275\sim 295}$ values, which corresponded to the large molecular weight of CDOM, consistent with other studies (Zhang and Qin 2007; Yacobi et al. 2003).

In this study, two components were grouped into the humic-like component by comparison with previously identified components (Table S2). This result does not suggest that only two types of fluorophores were present in these samples and does not suggest that both components were present in each sample of the two regions; it only means that humus-like substances were the main component of CDOM in this study area. C1 was likely derived from agricultural catchments, soil, or terrestrial/autochthonous sources, as reported in other widespread freshwater environments (Table S2, Stedmon et al. 2003; Stedmon and Markager 2005; Murphy et al. 2006; Murphy et al. 2008; Singh et al. 2010; Zhu et al. 2018). C2 resembled a microbial humic-like component and existed in forest, stream, rainwater, and wetland environments (Table S2, Stedmon et al. 2003; Cory and McKnight 2005; Williams et al. 2010; Cussa and Guéguenb 2012). Although the fluorescence components were similar, the average proportions of these fluorescence components (C1(%) and C2(%)) were different in the two regions, which might be due to the comprehensive effect in the two regions. In previous studies, strong relationships ($p < 0.01$) were observed between monthly mean net inflow runoff (Q_{net}) and the proportions of the fluorescence components (i.e., C2(%)), which suggested that Q_{net} influenced the CDOM in the fluvial plain Lake Taihu watershed (Zhou et al. 2018) and highly significant positive relationships were observed between the percentage of anthropogenic land use and C1 ($r^2 = 0.71$, $p < 0.001$) in drinking water reservoirs (Shi et al. 2020). Changes in the relative proportions of fluorescence components C1 and C2 are indicative of impacts of biogeochemical processes on CDOM dynamics (Pitta et al. 2016).

Possible sources of CDOM in TSYaR and TSYeR

According to a previous study (Coble 2007), the sources of CDOM components in aquatic ecosystems are mainly allochthonous (i.e., terrestrial) and autochthonous sources (i.e., microbial/algae). The allochthonous sources mainly result from higher animal and plant residues in the soils, which are degraded by bacteria and fungi, and most of them predominately show humic-like peaks; the autochthonous sources mainly result from biological activities such as plankton, aquatic bacteria, and algae in aquatic ecosystems, and those sources are mostly expressed as a protein-like peak (Kirk 2011; Zhang et al. 2011b).

Several related parameters of CDOM spectral absorption can be used to reflect the sources and components of CDOM, such as $SUVA_{254}$ and $S_{275-295}$. In addition to characterizing the absorption capacity of light, $SUVA_{254}$ can also be used to distinguish CDOM sources and types, which act as indicators of humus aromaticity and reactivity (Weishaar et al. 2003). This study showed the average $SUVA_{254}$ value of the two regions was $2.20 \pm 0.96 \text{ L}^{-1} \text{ m}^{-1} \text{ mg}$, which is relatively high

compared with some studies (Hu et al. 2017; Yang et al. 2019). Allochthonous sources are believed to be more aromatic than autochthonous sources (McKnight et al. 2001). Thus, the relatively high $SUVA_{254}$ value indicated a greater abundance of allochthonous sources in this study. The mean CDOM $S_{275-295}$ value was $17.19 \pm 1.86 \mu\text{m}^{-1}$, which was relatively low compared with that measured in some oceans and lakes (Pitta et al. 2016; Zhou et al. 2018). This result indicated that the allochthonous sources of humic compounds accounted for a large proportion in present study regions. In this study, especially in TSYeR, the $a_{\text{CDOM}(355)}$ and $SUVA_{254}$ values from the upper reaches of the Yellow River to the downstream roughly showed a decreasing trend (Fig. 3A, C), which revealed the input of terrestrial humus.

The fluorescence index (FI), biological index (BIX), and humification index (HIX) can also be used to analyze the structures and sources of CDOM. FI reflects the relative contribution of aromatic and non-aromatic amino acids to fluorescence intensity as an indicator of CDOM source and degradation (Cory and McKnight 2005). Studies have shown that an FI value > 1.9 indicates that CDOM is derived from the extracellular release of bacteria and algae and has significant endogenous production characteristics; an FI value < 1.4 reflects the origin of allochthonous sources such as terrestrial plants and soil organic matter (McKnight et al. 2001; Huguet et al. 2009). The FI in our study varied from 1.50 to 1.79, with a mean of 1.63 ± 0.07 , and the values were closer to 1.4 based on the distribution of all FI values. Compared with TSYaR, CDOM in TSYeR had stronger allochthonous characteristics. The biological index (BIX) is used to measure and indicate the proportion of self-generated contributions in CDOM. BIX ranged between 0.6 and 0.8, indicating that the self-generated source contribution was small; when the value exceeds 1.0, the degree of CDOM degradation is high, and the characteristics of the self-generated source components are obvious (Birdwell and Engel 2010). BIX was recorded in TSYaR (0.80 ± 0.01) in TSYeR (0.71 ± 0.03), which indicated that the endogenous contribution to the CDOM of the two source regions was small and reflected that the allochthonous sources of TSYeR were more abundant than those of TSYaR, consistent with the FI . The humification index (HIX) is directly proportional to the degree of organic matter humification; $HIX < 4$ is associated with autochthonous sources, and $HIX > 10$ indicates strongly humified organic material, mainly of terrestrial origin (Huguet et al. 2009; Vacher 2004). The HIX values in our study varied from 1.94 to 6.95, and the values were greater than 4 in most river segments. In particular, TSYeR showed terrestrial input except for individual sites (Fig. 5E, F). In summary, based on the comprehensive CDOM spectral absorption and fluorescence parameters, CDOM was mainly derived from externally input humus, and TSYeR showed stronger allochthonous sources in this study region.

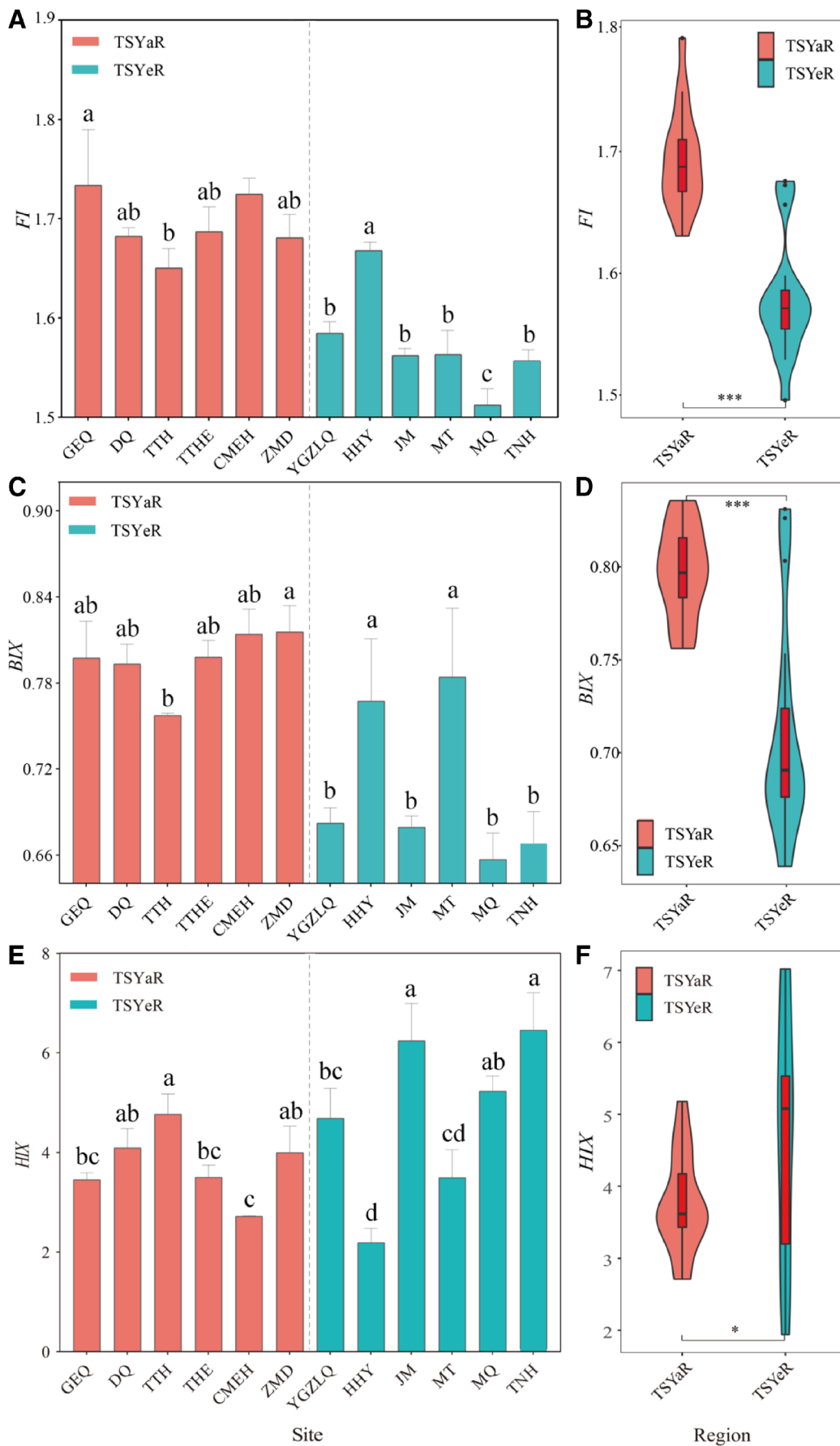


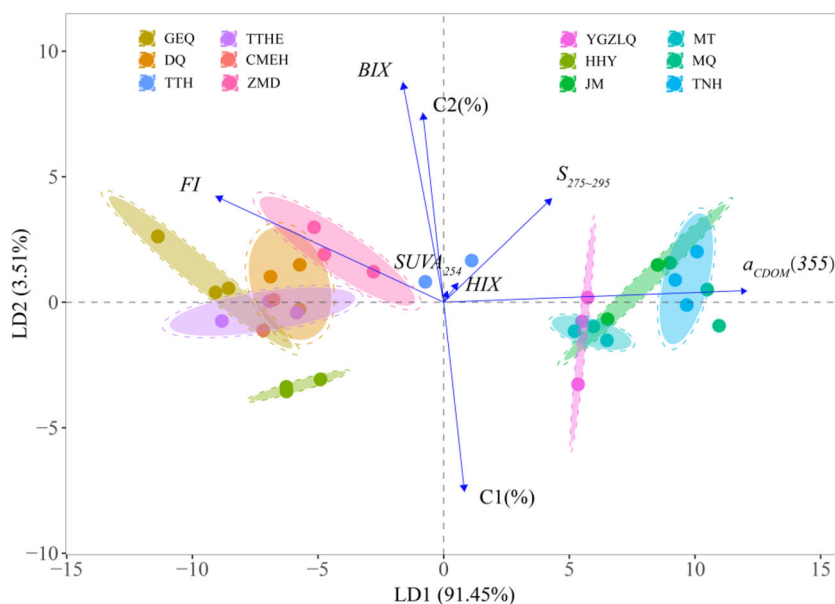
Fig. 5 Bar plots and vioplot box plots showed the spatial distribution fluorescence parameters in all sections and two regions of TSYaR and TSYeR, respectively. (A, B) spatial variation of fluorescence index (*FI*); (C, D) spatial variation of the biological index (*BLX*); (E, F) spatial variation of the humification index (*HIX*). Red box boundaries in vioplot box plots indicate the 25th and 75th percentiles; the whiskers represent the maximum/minimum values except for outliers; the inner horizontal blacked line is the median; the outside violin plot showed the data distribution and its probability density. Different lowercase letters above the bar plots mean significant difference at the 0.05 level. Single and double asterisks denote being statistically significant at the levels of 0.05 and 0.001, respectively

Relationship between CDOM and environmental variables in TSYaR and TSYeR

The concentration and composition of CDOM in different aquatic environments are mainly determined by factors such as soil type, vegetation type, runoff, rainfall, and human activities, which also indirectly affect biological sources such as aquatic plants, algae, bacteria, and microorganism degradation and secretion (Zhang et al. 2011b). Changes in land-use types in a river basin, such as agricultural farming, deforestation, and grassland degradation, which promote soil erosion, greatly increase the organic carbon output flux and the input of river humus (Shi et al. 2020). In our study, the soil type in TSYaR is mainly alpine steppe/frozen soils, and TSYeR is mainly alpine meadow soils; the vegetation coverage of TSYeR was significantly higher than that of TSYaR (Table S1). It is important to study the relationship between CDOM and water environment variables that play a crucial role in the carbon cycle of river ecosystems, the source and distribution of CDOM, and the impact of environmental factors on CDOM.

Some studies pointed out that CDOM responds well to climate change, trophic gradients, and anthropogenic disturbances, which are reflected in specific indexes such as storm events and increased precipitation, the trophic state index (TSI), and anthropogenic humic-like inputs (Ritson et al. 2014; Zhang et al. 2018; Zhou et al. 2019b). High turbidity limits the transmission of light in water and affects the photodegradation process of CDOM, which also indirectly affects the light absorption capacity of CDOM (Stedmon et al. 2007a; Zhang et al. 2011a). There were significant positive correlations between Turb and $a_{CDOM}(355)$ and $SUVA_{254}$ in the two regions. In addition, it was found that the WT, TN, NH_4^+-N , $a_{CDOM}(355)$, and $SUVA_{254}$ gradually increased with decreasing altitude, and there was a strong linear relationship between these variables ($p < 0.05$) in TSYeR (Fig. S1). This result is consistent with that between CDOM and nutrients in lake and river water (Hur and Cho 2012; Zhang et al. 2014). Water temperature affects the activity of microorganisms and the degradation of dissolved organic matter in water, further affecting the change in the concentration of CDOM (Zhou et al. 2019a; Boyd and Osburn 2004; Cole et al. 2011). The water source in TSYeR is mainly snow and melted ice from the north of Bayan Hara Mountain, rainfall, tributary inflow, and underground frozen soil water. Due to global warming, the rising temperature will inevitably lead to an increase in meltwater inflow in the source area and will also bring more external inputs through runoff. There were significant positive correlations between TP, nitrogen forms (TN, NH_4^+-N), and the CDOM absorption coefficients $a_{CDOM}(355)$ and $SUVA_{254}$ in TSYaR and TSYeR, respectively. In view of this, CDOM may be an important source of nutrients for the growth of phytoplankton in water (Kowalczyk et al. 2009). $NO_3^- - N$ had significant correlation with *HIX* ($r = -0.540$, $p < 0.05$)

Fig. 6 Biplot of linear discriminant analysis (LDA) for CDOM spectral parameters ($a_{CDOM}(355)$, $SUVA_{254}$, $S_{275-295}$, *FI*, *BLX*, *HIX*) and the fluorescence components percentage (*C1*(%) and *C2*(%)) in the twelve segments of the two regions



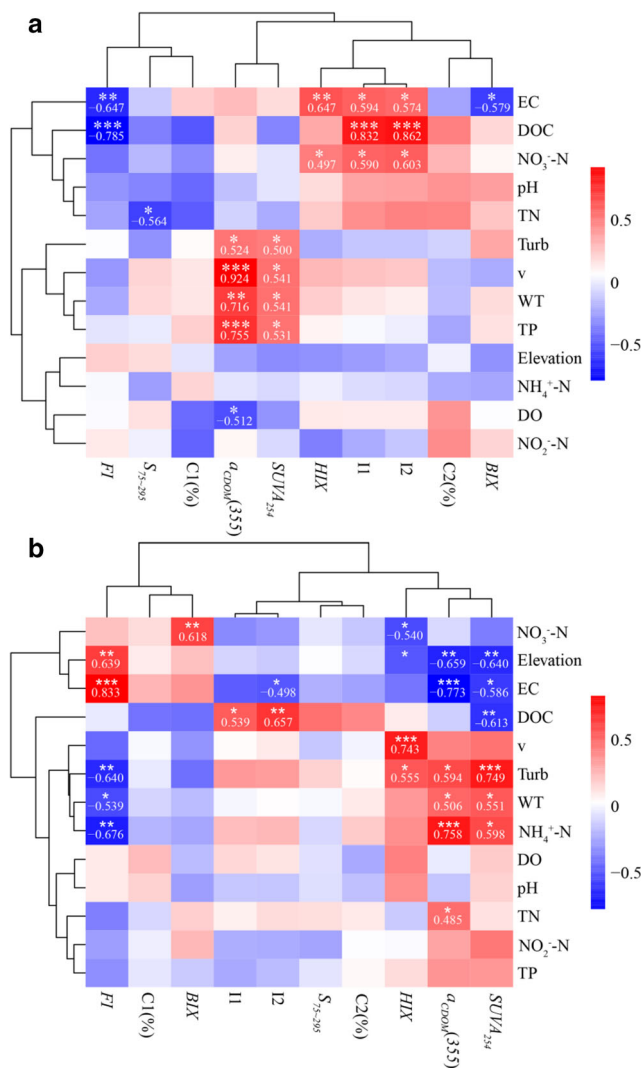


Fig. 7 Spearman's correlation analysis of CDOM absorption spectral parameters ($a_{CDOM}(355)$, $SUVA_{254}$, $S_{275-295}$), the fluorescence components percentage (C1(%) and C2(%)), the corresponding fluorescent intensity (I1 and I2) of the fluorescence component (C1 and C2), the fluorescence parameters (FI , BIX , HIX), and environmental variables (Elevation, WT, DO, EC, pH, v, Turb, DOC, TN, NO_3^- -N, NO_2^- -N, NH_4^+ -N, TP). Single asterisk indicates coefficients at 0.05 significance level, $p < 0.05$; Double asterisks indicate coefficients at 0.01 significance level, $p < 0.01$; Triple asterisks indicate coefficients at 0.001 significance level, $p < 0.001$

and BIX ($r = 0.618$, $p < 0.01$) in TSYeR (Fig. 7b). The activities of bacteria and microorganisms play an important role when they dominate the nitrification and degradation of organic matter.

The two regions were comprehensively studied, and the positive correlations between DOC concentrations and the corresponding fluorescence intensity indicated that humic-like fluorescence can adequately reflect the DOC concentration in rivers, which also indicated that the humic-like component was an important component of DOC (Fig. 7a, b; Fig. S2 [A, B]). There was a significant positive correlation between FI and EC in this study (Fig. 7a, b; Fig. S2 [C]). The

reason may be that the structure and morphology of humic-like substances are affected by water ions, further affecting their fluorescence features (Chen et al. 2007; Zhao et al. 2017). Temperature plays an important role in the composition and spectral characteristics of CDOM by affecting some biochemical processes, such as nitrogen cycling and microbially mediated tundra soil carbon decomposition (Zhou et al. 2019a; Feng et al. 2020). In this study, WT and $a_{CDOM}(355)$ ($r^2 = 0.6416$, $p < 0.001$) and $SUVA_{254}$ ($r^2 = 0.5335$, $p < 0.001$) showed significant linear correlations. The quality of the water environment was relatively good in this study area. For water bodies with heavy pollution and high trophic states or CDOM is mainly generated by internal sources, our results may produce some errors or uncertainties if applied. In addition, the potential weakness is that the number and frequency of samples in the study regions have certain influences and limitations on the research results. In the future, we will collect data at a higher frequency and a larger watershed scale and will also conduct in-depth research on the relationship and mechanism between CDOM and environmental variables under extreme events such as heavy rainfall and floods.

Conclusions

The CDOM absorption spectra of the source regions of the Yangtze and Yellow Rivers had a high degree of consistency, and the average absorption coefficient of TSYeR was significantly higher than that of TSYaR at wavelengths less than 643 nm ($p < 0.05$). Two fluorescence components (C1 and C2) were identified and grouped into one category: humic-like components using EEMs and the PARAFAC model; these components had highly similar (excitations/emission) max positions in the two regions. CDOM spectral absorption ($SUVA_{254}$, $S_{275-295}$) and fluorescence parameters (FI , BIX , HIX) indicated that the contribution of the allochthonous source to the CDOM of the two source regions was large and that the terrestrial humus input of the TSYeR was higher than that of the TSYaR. Multivariate analyses showed the relationship between CDOM spectral parameters and environmental variables. The positive correlations between DOC concentrations and fluorescence intensity indicated that humic-like fluorescence can accurately reflect the DOC concentration in rivers, and that the humic-like component was an important component of DOC in this study. There were significant positive correlations between TP, nitrogen forms (TN, NH_4^+ -N), and $a_{CDOM}(355)$ and $SUVA_{254}$ in TSYaR and TSYeR, respectively. In particular, the WT gradually increased with the decrease in altitude in TSYeR, and due to global warming, the rising temperature may lead to an increase in meltwater inflow in the source area and will also result in more external organic inputs.

Acknowledgments The authors sincerely thank all staff and students that helped with CDOM field sampling. We also greatly appreciate Dr. Wei Zhang from Shanghai Ocean University and Dr. Liang Chen from Xi'an University of Technology for their revision and suggestions. We would like to express our deep thanks to Prof. Céline Guéguen for editorial assistance. The authors are grateful to the two anonymous reviewers for their very constructive comments.

Funding information This work was jointly supported by the National Natural Science Foundation of China (No. 51939009, No. 51622901, No. 51709225).

References

- Andersen CM, Bro R (2003) Practical aspects of PARAFAC modeling of fluorescence excitation-emission data. *J Chemom* 17(4):200–215
- Baker A (2002) Fluorescence properties of some farm wastes: implications for water quality monitoring. *Water Res* 36(1):189–195
- Birdwell JE, Engel AS (2010) Characterization of dissolved organic matter in cave and spring waters using UV–Vis absorbance and fluorescence spectroscopy. *Org Geochem* 41(3):270–280
- Blue B, Brierley G, Yu GA (2013) Geodiversity in the Yellow River source zone. *J Geogr Sci* 23(5):775–792
- Boyd TJ, Osburn CL (2004) Changes in CDOM fluorescence from allochthonous and autochthonous sources during tidal mixing and bacterial degradation in two coastal estuaries. *Mar Chem* 89(1–4):189–210
- Bricaud A, Morel A, Prieur L (1981) Absorption by dissolved organic matter of the sea (yellow substance) in the UV and visible domains. *Limnol Oceanogr* 26(1):43–53
- Bro R (1997) PARAFAC. Tutorial and applications. *Chemom Intell Lab Syst* 38(2):149–171
- Burdige DJ, Kline SW, Chen WH (2004) Fluorescence dissolved organic matter in marine sediment pore waters. *Mar Chem* 89(1–4):289–311
- Cai HY, Yang XH, Xu XL (2015) Human-induced grassland degradation/restoration in the central Tibetan Plateau: the effects of ecological protection and restoration projects. *Ecol Eng* 83:112–119
- Chen CL, Wang XK, Jiang H, Hu WP (2007) Direct observation of macromolecular structures of humic acid by AFM and SEM. *Colloids Surf A Physicochem Eng Asp* 302(1–3):121–125
- Coble PG (2007) Marine optical biogeochemistry: the chemistry of ocean color. *Chem Rev* 107(2):402–418
- Cole JJ, Carpenter SR, Kitchell J, Pace ML, Solomon CT, Weidel B (2011) Strong evidence for terrestrial support of zooplankton in small lakes based on stable isotopes of carbon, nitrogen, and hydrogen. *PNAS* 108(5):1975–1980
- Cory RM, Mcknight DM (2005) Fluorescence spectroscopy reveals ubiquitous presence of oxidized and reduced quinones in dissolved organic matter. *Environ Sci Technol* 39(21):8142–8149
- Cussa CW, Guéguen C (2012) Determination of relative molecular weights of fluorescence components in dissolved organic matter using asymmetrical flow field-flow fractionation and parallel factor analysis. *Anal Chim Acta* 733:98–102
- Ding ZY, Wang YY, Lu RJ (2018) An analysis of changes in temperature extremes in the Three River Headwaters Region of the Tibetan Plateau during 1961–2016. *Atmos Res* 209:103–114
- Doxaran D, Froidefond JM, Lavender S, Castaing P (2002) Spectral signature of highly turbid waters: application with spot data to quantify suspended particulate matter concentrations. *Remote Sens Environ* 81(1):149–161
- Fang YP (2013) Managing the Three-Rivers Headwater Region, China: from ecological engineering to social engineering. *AMBIO* 42(5):566–576
- Fang YP, Qin DH, Ding YJ (2011) Frozen soil change and adaptation of animal husbandry: a case of the source regions of Yangtze and Yellow Rivers. *Environ Sci Pol* 14(5):555–568
- Feng JL, Hu PT, Su XF, Li QL, Sun JH, Li YF (2018) Impact of suspended sediment on the behavior of polycyclic aromatic hydrocarbons in the Yellow River: spatial distribution, transport and fate. *Appl Geochem* 98:278–285
- Feng JJ, Wang C, Lei JS, Yang YF, Yan QY, Zhou XS et al (2020) Warming-induced permafrost thaw exacerbates tundra soil carbon decomposition mediated by microbial community. *Microbiome* 8(1):1–12
- Grand-Clement E, Luscombe DJ, Anderson K, Gatis N, Benaud P, Brazier RE (2014) Antecedent conditions control carbon loss and downstream water quality from shallow, damaged peatlands. *Sci Total Environ* 493:961–973
- Granéli E, Carlsson P, Legrand C (1999) The role of C, N and P in dissolved and particulate organic matter as a nutrient source for phytoplankton growth, including toxic species. *Aquat Ecol* 33(1):17–27
- Green SA, Blough NV (1994) Optical absorption and fluorescence properties of chromophoric dissolved organic matter in natural waters. *Limnol Oceanogr* 39(8):1903–1916
- Hassett JP (2006) Chemistry: enhanced: dissolved natural organic matter as a microreactor. *Science* 311(5768):1723–1724
- Helms JR, Stubbins A, Ritchie JD, Minor EC, Kieber D, Mopper K (2008) Absorption spectral slopes and slope ratios as indicators of molecular weight, source, and photobleaching of chromophoric dissolved organic matter. *Limnol Oceanogr* 53(3):955–969
- Hu B, Wang PF, Qian J, Wang C, Zhang NN, Cui XA (2017) Characteristics, sources, and photobleaching of chromophoric dissolved organic matter (CDOM) in large and shallow Hongze Lake, China. *J Great Lakes Res* 43(6):1165–1172
- Hudson N, Baker A, Reynolds D (2007) Fluorescence analysis of dissolved organic matter in natural, waste and polluted waters—a review. *River Res Appl* 23(6):631–649
- Huguet A, Vacher L, Relexans S, Froidefond JM, Parlanti E (2009) Properties of fluorescence dissolved organic matter in the Gironde Estuary. *Org Geochem* 40(6):706–719
- Huovinen PS, Penttölä H, Soimasuo MR (2003) Spectral attenuation of solar ultraviolet radiation in humic lakes in Central Finland. *Chemosphere* 51(3):205–214
- Hur J, Cho J (2012) Prediction of BOD, COD, and total nitrogen concentrations in a typical urban river using a fluorescence excitation-emission matrix with PARAFAC and UV absorption indices. *Sensors* 12:972–986
- Jiang C, Zhang LB, Tang ZP (2017) Multi-temporal scale changes of streamflow and sediment discharge in the headwaters of Yellow River and Yangtze River on the Tibetan Plateau, China. *Ecol Eng* 102:240–254
- Jørgensen L, Stedmon CA, Granskog MA, Middelboe M (2014) Tracing the long-term microbial production of recalcitrant fluorescence dissolved organic matter in seawater. *Geophys Res Lett* 41(7):2481–2488
- Kensuke K, Tsuyoshi A, Hiro-omi Y, Tsutsumi M, Yasuda T, Watanabe O, Wang SP (2005) Comparing MODIS vegetation indices with AVHRR NDVI for monitoring the forage quantity and quality in Inner Mongolia grassland China. *Grassl Sci* 51(1):33–40
- Kirk JTO (2011) Light and photosynthesis in aquatic ecosystem, 3rd edn. Cambridge University Press, Cambridge, pp 53–70
- Kowalczyk P, Durako MJ, Young H, Kahn AE, Cooper WJ, Gonsior M (2009) Characterization of dissolved organic matter fluorescence in the South Atlantic Bight with use of PARAFAC model: interannual variability. *Mar Chem* 113(3–4):182–196

- Lapierre JF, Frenette JJ (2009) Effects of macrophytes and terrestrial inputs on fluorescence dissolved organic matter in a large river system. *Aquat Sci* 71(1):15–24
- Li PH, Hur J (2017) Utilization of uv-vis spectroscopy and related data analyses for dissolved organic matter (dom) studies: a review. *Crit Rev Environ Sci Technol* 47(3):131–154
- Li ZW, Wang ZY, Pan BZ, Du J, Brierley G, Yu GA, Blue B (2013) Analysis of controls upon channel planform at the first great bend of the upper Yellow River, Qinghai-Tibet Plateau. *J Geogr Sci* 23(5):833–848
- Li SJ, Ju HY, Ji MC, Zhang JQ, Song KS, Chen P (2018a) Terrestrial humic-like fluorescence peak of chromophoric dissolved organic matter as a new potential indicator tracing the antibiotics in typical polluted watershed. *J Environ Manag* 228:65–76
- Li ZW, Wu YZ, Hu XY, Zhou YJ, Yan X (2018b) Morphological features and spatial-temporal change of braided reach of Tongtian River in the Yangtze River source region. *J Yangtze River Sci Res Inst* 35(9):6–11 (in Chinese)
- Liu JY, Shao QQ, Fan JW (2013) Ecological construction achievements assessment and its revelation of ecological project in Three rivers Headwaters Region. *Chin J Nat* 35(1):40–46
- Liu XF, Zhang JS, Zhu XF, Pan YZ, Liu YX, Zang DH, Lin ZH (2014) Spatiotemporal changes in vegetation coverage and its driving factors in the Three-River Headwaters Region during 2000–2011. *J Geogr Sci* 24(2):288–302
- Loiselle SA, Bracchini L, Dattilo AM, Ricci M, Tognazzi A, Cózar A, Rossi C (2009) The optical characterization of chromophoric dissolved organic matter using wavelength distribution of absorption spectral slopes. *Limnol Oceanogr* 54(2):590–597
- McKnight DM, Boyer EW, Westerhoff PK, Doran PT, Kulbe T, Andersen DT (2001) Spectrofluorometric characterization of dissolved organic matter for indication of precursor organic material and aromaticity. *Limnol Oceanogr* 46(1):38–48
- Meng FC, Su FG, Yang DQ, Tong K, Hao ZC (2016) Impacts of recent climate change on the hydrology in the source region of the Yellow River basin. *J Hydrol* 6:66–81
- Morris DP, Hargreaves BR (1997) The role of photochemical degradation of dissolved organic carbon in regulating the UV transparency of three lakes on the Pocono plateau. *Limnol Oceanogr* 42(2):239–249
- Murphy KR, Ruiz GM, Dunsmuir WTM, Waite TD (2006) Optimized parameters for fluorescence-based verification of ballast water exchange by ships. *Environ Sci Technol* 40(7):2357–2362
- Murphy KR, Stedmon CA, Waite TD, Ruiz GM (2008) Distinguishing between terrestrial and autochthonous organic matter sources in marine environments using fluorescence spectroscopy. *Mar Chem* 108(1–2):40–58
- Murphy KR, Stedmon CA, Graeber D, Bro R (2013) Fluorescence spectroscopy and multi-way techniques. *PARAFAC*. *Anal Methods* 5(23):6557–6566
- National Bureau of Environment Protection Editor (2002) Water and wastewater monitoring analysis methods, 4th edn. Chinese Environment Science press, Beijing (in Chinese)
- Nima C, Hamre B, Frette Ø, Erga SR, Chen YC, Zhao L et al (2016) Impact of particulate and dissolved material on light absorption properties in a high-altitude lake in Tibet, China. *Hydrobiologia* 768(1):63–79
- Osburn CL, Retamal L, Vincent WF (2009) Photoreactivity of chromophoric dissolved organic matter transported by the Mackenzie River to the Beaufort Sea. *Mar Chem* 115(1):10–20
- Pan BZ, Wang ZY, Li ZW, Yu GA, Xu MZ, Zhao N, Brierley G (2013) An exploratory analysis of benthic macroinvertebrates as indicators of the ecological status of the upper yellow and Yangtze rivers. *J Geogr Sci* 23(5):871–882
- Pirmia A, Golshan M, Darabi H, Adamowski J, Rozbeh S (2019) Using the Mann–Kendall test and double mass curve method to explore stream flow changes in response to climate and human activities. *J Water Clim Chang* 10(4):725–742
- Pitta E, Zeri C, Tzortziou M, Mousdisc G, Scoullod M (2016) Seasonal variations in dissolved organic matter composition using absorbance and fluorescence spectroscopy in the Dardanelles Straits–North Aegean Sea mixing zone. *Cont Shelf Res* 149:82–95
- Qian J, Wang GX, Ding YJ, Liu SY (2006) The land ecological evolutionary patterns in the source areas of the Yangtze and Yellow Rivers in the past 15 years, China. *Environ Monit Assess* 116(1–3):137–156
- Raymond PA, Oh NH, Turner RE, Broussard W (2008) Anthropogenically enhanced fluxes of water and carbon from the Mississippi River. *Nature* 451(7177):449–452
- Regnier P, Friedlingstein P, Ciais P, Mackenzie FT, Gruber N, Janssens IA et al (2013) Anthropogenic perturbation of the carbon fluxes from land to ocean. *Nat Geosci* 6(8):597–607
- Ritson JP, Graham NJD, Templeton MR, Clark JM, Gough R, Freeman C (2014) The impact of climate change on the treatability of dissolved organic matter (DOM) in upland water supplies: a UK perspective. *Sci Total Environ* 473–474:714–730
- Rochelle-Newall EJ, Fisher TR (2002) Chromophoric dissolved organic matter and dissolved organic carbon in Chesapeake Bay. *Mar Chem* 77(1):23–41
- Scheffuß E, Eglinton TI, Spencer-Jones CL, Rullkötter J, De Pol-Holz R, Talbot HM et al (2016) Hydrologic control of carbon cycling and aged carbon discharge in the Congo River basin. *Nat Geosci* 9(9):687–690
- Seritti A, Russo D, Nannicini L, Del Vecchio R (1998) DOC, absorption and fluorescence properties of estuarine and coastal waters of the Northern Tyrrhenian Sea. *Chem Speciat Bioavailab* 10(3):95–106
- Shang YX, Song KS, Jiang P, Ma JH, Wen ZD, Zhao Y (2018) Optical absorption properties and diffuse attenuation of photosynthetic active radiation for inland waters across the Tibetan Plateau. *J Lake Sci* 30(3):802–811 (in Chinese)
- Shao QQ, Cao W, Fan JW, Huang L, Xu XL (2017) Effects of an ecological conservation and restoration project in the Three-River Source Region, China. *J Geogr Sci* 27(2):183–204
- Shen ZL, Liu Q, Zhang SM (2003) Distribution, variation and removal patterns of total nitrogen and organic nitrogen in the changjiang river. *Oceanol Limnol Sin* 34(6):577–585 (in Chinese)
- Sheng WP, Zhen L, Xiao Y, Hu YF (2019) Ecological and socioeconomic effects of ecological restoration in China's Three Rivers Source Region. *Sci Total Environ* 650:2307–2313
- Shi HY, Li TJ, Wei JH (2017) Evaluation of the gridded CRU TS precipitation dataset with the point raingauge records over the Three-River Headwaters Region. *J Hydrol* 548:322–332
- Shi Y, Zhang LQ, Li YP, Zhou L, Zhou YQ, Zhang YL, Huang C, Li H, Zhu G (2020) Influence of land use and rainfall on the optical properties of dissolved organic matter in a key drinking water reservoir in China. *Sci Total Environ* 699:134301
- Singh S, D'Sa EJ, Swenson EM (2010) Chromophoric dissolved organic matter (CDOM) variability in Barataria basin using excitation–emission matrix (EEM) fluorescence and parallel factor analysis (PARAFAC). *Sci Total Environ* 408(16):3211–3222
- Stedmon CA, Bro R (2008) Characterizing dissolved organic matter fluorescence with parallel factor analysis: a tutorial. *Limnol Oceanogr Methods* 6(11):572–579
- Stedmon CA, Markager S (2003) Behaviour of the optical properties of coloured dissolved organic matter under conservative mixing. *Estuar Coast Shelf Sci* 57(5–6):973–979

- Stedmon CA, Markager S (2005) Tracing the production and degradation of autochthonous fractions of dissolved organic matter by fluorescence analysis. *Limnol Oceanogr* 50(5):1415–1426
- Stedmon CA, Markager S, Kaas H (2000) Optical properties and signatures of chromophoric dissolved organic matter (CDOM) in danish coastal waters. *Estuar Coast Shelf Sci* 51(2):267–278
- Stedmon CA, Markager S, Bro R (2003) Tracing dissolved organic matter in aquatic environments using a new approach to fluorescence spectroscopy. *Mar Chem* 82(3–4):239–254
- Stedmon CA, Markager S, Tranvik L, Kronberg L, Slätisc T, Martinsena W (2007a) Photochemical production of ammonium and transformation of dissolved organic matter in the Baltic Sea. *Mar Chem* 104(3–4):227–240
- Stedmon CA, Thomas DN, Granskog M, Kaartokallio H, Papadimitriou S, Kuosa H (2007b) Characteristics of dissolved organic matter in Baltic coastal sea ice: allochthonous or autochthonous origins? *Environ Sci Technol* 41(21):7273–7279
- Stets EG, Striegl RG (2012) Carbon export by rivers draining the conterminous United States. *Inland Waters* 2(4):177–184
- Tranvik LJ, Downing JA, Cotner JB, Loiselle SA, Striegl RG, Ballatore TJ et al (2009) Lakes and reservoirs as regulators of carbon cycling and climate. *Limnol Oceanogr* 54(6):2298–2314
- Vacher L. (2004) Etude par fluorescence des propriétés de la matière organique dissoute dans les systèmes estuariens. Cas des estuaires de la Gironde et de la Seine, PhD thesis, Université Bordeaux I, 255
- Vahatalo AV, Wetzel RG, Paerl HW (2005) Light absorption by phytoplankton and chromophoric dissolved organic matter in the grain-age basin and estuary of the Neuse River, North Carolina (U.S.A.). *Freshw Biol* 50(3):477–493
- Veuger B, Middelburg JJ, Boschker HTS, Nieuwenhuize J, Rijswijk PV (2004) Microbial uptake of dissolved organic and inorganic nitrogen in Randers Fjord. *Estuar Coast Shelf Sci* 61(3):507–515
- Wan W, Xiao PF, Feng XZ, Li H, Ma RH, Duan HT, Zhao L (2014) Monitoring lake changes of Qinghai-Tibetan Plateau over the past 30 years using satellite remote sensing data. *Chin Sci Bull* 59(10):1021–1035
- Wang GX, Li Q, Cheng GD, Shen YP (2001) Climate change and its impact on the eco-environment in the source regions of the Yangtze and Yellow Rivers in recent 40 years. *J Glaciol Geocryol* 23(4):346–352 (in Chinese)
- Wang YS, Cheng CC, Xie Y, Liu BY, Yin SQ, Liu YN, Hao Y (2017) Increasing trends in rainfall-runoff erosivity in the source region of the three rivers, 1961–2012. *Sci Total Environ* 592:639–648
- Wehrli B (2013) Biogeochemistry: conduits of the carbon cycle. *Nature* 503(7476):346–347
- Weishaar JL, Aiken GR, Bergamaschi BA, Fram MS, Fujii R, Mopper K (2003) Evaluation of specific ultraviolet absorbance as an indicator of the chemical composition and reactivity of dissolved organic carbon. *Environ Sci Technol* 37(20):4702–4708
- Williams CJ, Yamashita Y, Wilson HF, Jaffé R, Xenopoulos MA (2010) Unraveling the role of land use and microbial activity in shaping dissolved organic matter characteristics in stream ecosystems. *Limnol Oceanogr* 55(3):1159–1171
- Williams CJ, Frost PC, Morales-Williams AM, Larson JH, Richardson WB, Chiandret AS, Xenopoulos MA (2016) Human activities cause distinct dissolved organic matter composition across freshwater ecosystems. *Glob Chang Biol* 22(2):613–626
- Wu SS, Yao ZJ, Huang HQ, Liu ZF, Chen YS (2013) Glacier retreat and its effect on stream flow in the source region of the Yangtze River. *J Geogr Sci* 23(5):849–859
- Wu XL, Zhang X, Xiang XH, Zhang K, Jin HJ, Chen X, Wang C, Shao Q, Hua W (2018) Changing runoff generation in the source area of the Yellow River: mechanisms, seasonal patterns and trends. *Cold Reg Sci Technol* 155:58–68
- Xia L, Pan JY, Adam D (2018) Mixing behavior of chromophoric dissolved organic matter in the Pearl River Estuary in spring. *Cont Shelf Res* 154:46–54
- Xu J, Fang CY, Gao D, Zhang HS, Gao C, Xu ZC, Wang Y (2018a) Optical models for remote sensing of chromophoric dissolved organic matter (CDOM) absorption in Poyang Lake [J]. *ISPRS J Photogramm Remote Sens* 142:124–136
- Xu M, Kang SC, Chen XL, Wu H, Wang XY, Su ZB (2018b) Detection of hydrological variations and their impacts on vegetation from multiple satellite observations in the Three-River Source Region of the Tibetan Plateau. *Sci Total Environ* 639:1220–1232
- Yacobi YZ, Alberts JJ, Takács M, McElvaine ML (2003) Absorption spectroscopy of colored dissolved organic carbon in Georgia (USA) rivers: the impact of molecular size distribution. *J Limnol* 62(1):41–46
- Yang LY, Chen W, Zhuang WE, Cheng Q, Li WX, Wang H, Guo W, Chen CTA, Liu M (2019) Characterization and bioavailability of rainwater dissolved organic matter at the southeast coast of China using absorption spectroscopy and fluorescence EEM-PARAFAC. *Estuar Coast Shelf Sci* 217:45–55
- Yu GA, Liu L, Li ZW, Li YF, Huang HQ, Brierley G, Blue B, Wang ZY, Pan BZ (2013) Fluvial diversity in relation to valley setting in the source region of the Yangtze and Yellow Rivers. *J Geogr Sci* 23(5):817–832
- Yu GA, Brierley G, Huang HQ, Wang ZY, Blue B, Ma YX (2014) An environmental gradient of vegetative controls upon channel planform in the source region of the Yangtze and Yellow Rivers. *Catena* 119:143–153
- Zhang YL, Qin BQ (2007) Feature of CDOM and its possible source in Meiliang bay and Da Taihu Lake in summer and winter. *Adv Water Sci* 18(3):415–423 (in Chinese)
- Zhang YL, Qin BQ, Zhu GW, Zhang L, Yang LY (2007a) Chromophoric dissolved organic matter (CDOM) absorption characteristics in relation to fluorescence in Lake Taihu, China, a large shallow subtropical lake. *Hydrobiologia* 581(1):43–52
- Zhang YL, Zhang EL, Liu ML, Wang X, Qin BQ (2007b) Variation of chromophoric dissolved organic matter and possible attenuation depth of ultraviolet radiation in Yunnan Plateau lakes. *Limnology* 8(3):311–319
- Zhang YL, Liu ML, Qin BQ, Feng S (2009) Photochemical degradation of chromophoric-dissolved organic matter exposed to simulated UV-B and natural solar radiation. *Hydrobiologia* 627(1):159–168
- Zhang YL, Yan Y, Zhang EL, Zhu GW, Liu ML, Feng LQ, Qin BQ, Liu XH (2011a) Spectral attenuation of ultraviolet and visible radiation in lakes in the Yunnan Plateau, and the middle and lower reaches of the Yangtze River, China. *Photochem Photobiol Sci* 10(4):469–482
- Zhang YL, Yin Y, Feng LQ, Zhu GW, Shi ZQ, Liu XH, Zhang Y (2011b) Characterizing chromophoric dissolved organic matter in Lake Tianmuhu and its catchment basin using excitation-emission matrix fluorescence and parallel factor analysis. *Water Res* 45(16):5110–5122
- Zhang YL, Gao G, Shi K, Niu C, Zhou YQ, Qin BQ, Liu X (2014) Absorption and fluorescence characteristics of rainwater CDOM and contribution to Lake Taihu, China. *Atmos Environ* 98:483–491
- Zhang YL, Zhou YQ, Shi K, Qin BQ, Yao XL, Zhang YB (2018) Optical properties and composition changes in chromophoric dissolved organic matter along trophic gradients: implications for monitoring and assessing lake eutrophication. *Water Res* 131:255–263
- Zhao Y, Song KS, Wen ZD, Fang C, Shang YX, Lv LL (2017) Evaluation of CDOM sources and their links with water quality in

- the lakes of Northeast China using fluorescence spectroscopy. *J Hydrol* 550:80–91
- Zhou YQ, Yao XL, Zhang YL, Shi K, Zhang Y, Jeppesen E, Gao G, Zhu G, Qin B (2017) Potential rainfall-intensity and pH-driven shifts in the apparent fluorescence composition of dissolved organic matter in rainwater. *Environ Pollut* 224:638–648
- Zhou YQ, Yao XL, Zhang YL, Shi K, Tang XM, Qin BQ et al (2018) Response of dissolved organic matter optical properties to net inflow runoff in a large fluvial plain lake and the connecting channels. *Sci Total Environ* 639:876–887
- Zhou L, Zhou YQ, Hu Y, Cai J, Liu X, Bai CR, Tang X, Zhang Y, Jang KS, Spencer RGM, Jeppesen E (2019a) Microbial production and consumption of dissolved organic matter in glacial ecosystems on the Tibetan Plateau. *Water Res* 160:18–28
- Zhou YQ, Li Y, Yao XL, Ding WH, Zhang YB, Erik J et al (2019b) Response of chromophoric dissolved organic matter dynamics to tidal oscillations and anthropogenic disturbances in a large subtropical estuary. *Sci Total Environ* 662:769–778
- Zhu WZ, Zhang J, Yang GP (2018) Mixing behavior and photobleaching of chromophoric dissolved organic matter in the Changjiang River estuary and the adjacent East China Sea. *Estuar Coast Shelf Sci* 207: 422–435

Publisher's note Springer Nature remains neutral with regard to jurisdictional claims in published maps and institutional affiliations.